DOI: 10.1002/ejic.200700891

Structural Aspects of the Growth Mechanism of Copper Nanoparticles Inside Apoferritin

Marcelo Ceolín,*[a] Natividad Gálvez,[b] Purificación Sánchez,[b] Belén Fernández,[b] and José M. Domínguez-Vera*[b]

Keywords: Copper nanoparticles / Apoferritin / X-ray absorption spectroscopy / Small-angle X-ray scattering

It is well known that some of the metal ions remain bound to apoferritin when incubating apoferritin with metal ions. In this study a structural insight, from X-ray absorption spectroscopy (XAS) and small angle X-ray scattering (SAXS) experiments, into the mechanism of inorganic core formation is presented. The results indicate that, in the case of Cu^{II} at pH 8, the metal ions bound to apoferritin are in fact Cu^{II} oxide/hydroxide. This Cu^{II} species does not react with the Cu^{II}-specific TTMAPP, traditionally used to detect Cu^{II}, because TTMAPP is too large to penetrate the apoferritin channel and interact with the metal ions. EXAFS results suggest that the Cu^{II} precursor can be described as an amorphous network of oxygen/hydroxide-coordinating polyhedra surrounding the copper ions. XAS results demonstrate that this Cu^{II}-oxide/hydroxide species is completely converted into zero-valent Cu nanoparticles when treated with $NaBH_4$. Furthermore, a structural model for the final Cu^0 nanoparticle is offered.

Introduction

Over the last few years considerable research efforts have focused on the preparation of water-soluble metallic nanoparticles for their use in biomedical applications.[1,2] Numerous physical and chemical methods have been employed to produce metallic nanoparticles focusing on the tight control of particle size and shape. Because of the strong dependence of the properties on particle size and shape on the nanometer scale, methods yielding uniformly sized and shaped nanoparticles have become extremely important. One possible route for obtaining nonaggregated water-soluble metallic nanoparticles is the use of a preorganized molecular matrix as a chemical and spatial nanocage for their construction. A typical example of this type of molecule is the iron storage oligomeric protein apoferritin,[3–7] considered as a model for other nanocavity-containing macromolecules such as virus capsides.[8] Apoferritin consists of a spherical protein shell composed of 24 subunits surrounding an aqueous cavity with a diameter of about 8 nm.[9,10] Channels are generated by the multi subunit construction of the apoferritin shell. Eight hydrophilic channels of about 4 Å allow the passage of metal ions and molecules of sufficiently small size into the cavity of the protein.[11]

[a] Instituto de Investigaciones Físico-Químicas Teóricas y Aplicadas, Universidad Nacional de La Plata and Consejo Nacional de Investigaciones Científicas y Tecnológicas, Diag. 113 y 64, 1900 La Plata, Argentine
E-mail: mrceolin@yahoo.com.ar
[b] Departamento de Química Inorgánica, Facultad de Ciencias, Universidad de Granada, 18071 Granada, Spain
E-mail: josema@ugr.es

The first approach to produce apoferritin-encapsulated metallic nanoparticles was the use of the apoferritin cavity for biomimetic oxidative hydrolysis reactions, producing apoferritins that are reconstituted with non-native inorganic compounds, usually in the form of oxides or oxyhydroxides.[12–15] A more recent approach is based on the high affinity of some metal ions for the apoferritin cavity[16] and on the capacity of these bonded metal ions to react with an appropriate reagent to produce a metallic particle, constrained to the size of the cavity.[17] Apoferritin has been reported to bind metal ions in its cavity at specific sites, with stoichiometric binding not higher than 60 atoms per apoferritin at pH 7.4.[16] However, the number of metal ions strongly increases when working at a higher pH. For example, when horse spleen apoferritin is treated with Cu^{II}, Co^{II} or Ni^{II} and the pH is dynamically adjusted to 8 the number of metal ions per apoferritin reaches values of about 300.[18,19] It has recently been reported that this route can be extended to the preparation of apoferritin-encapsulated Cu,[17,20] Co, Ni[18] and Pd.[21]

Douglas et al. found the existence of an electrostatic negative potential gradient directed toward the cavity of the ferritin, supporting the idea of positive ion encapsulation.[22] These encapsulated metal(II)–apoferritins are susceptible to reaction with an appropriate reductant to give rise to the nucleation and growth of a new $metal^0$–apoferritin nanoparticle.[18,19] Recently, our group reported that this route could be extended to the preparation of apoferritin-encapsulated Cu, Co and Ni nanoparticles from a previous apoferritin-encapsulated metal ion solution. The advantage of our procedure lies in the fact that we succeeded in isolat-

ing the metal(II) ion-loaded apoferritin species (Cu^{II}–apoferritin, Scheme 1), which, in a second step, can act as a nanoprecursor for the preparation of apoferritin-capsulated zero-valent metal nanoparticles, avoiding any precipitation outside the apoferritin protein.[18,19]

However, the chemical nature and structure of the apoferritin-encapsulated metal ions remained uncertain. Unfortunately, no X-ray powder or electron diffraction could be obtained to determine the structure of the encapsulated material.

In the present work we performed small angle X-ray scattering (SAXS), X-ray near edge structure (XANES) and extended X-ray absorption fine structure (EXAFS) experiments on the intermediate species (Cu^{II}–apoferritin) as well as the final product obtained after chemical reduction (Cu^0–apoferritin). The results obtained point out that the encapsulated-Cu^{II} metal ions are in fact a Cu-oxide/hydroxide apoferritin species and that it is completely transformed to a Cu zero-valent metal apoferritin after reduction with $NaBH_4$ (Scheme 1).

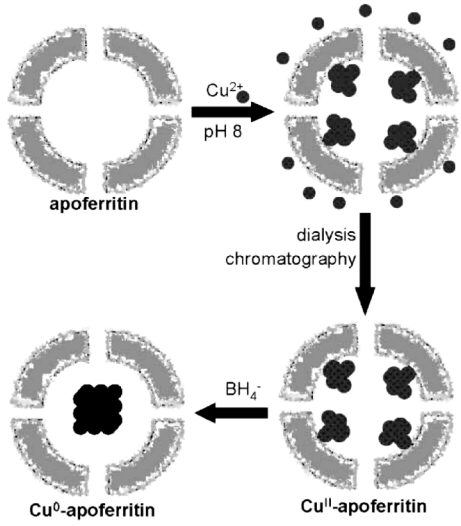

Scheme 1. Structure of apoferritin and schematic representation of the preparation of Cu^{II}– and Cu^0–apoferritin nanoparticles.

Results and Discussion

Apoferritin and Cu^{II} were incubated at pH 8 for 24 h. The resulting solution was exhaustively dialyzed against milli-Q water for two days to remove the Cu^{II} ions that were not bound to the protein. The apoferritin-containing fractions were isolated by G-25 Sephadex chromatography.

Apoferritin was monitored by UV/Vis spectroscopy at 280 nm and Cu by atomic absorption. The coelution of apoferritin and the metal (Figure 1, A) demonstrates that metal ions are attached to apoferritin. In addition, native apoferritin and Cu^{II}–apoferritin were electrophoretically analyzed on polyacrylamide gel (PAGE), under native (non-denaturing) conditions (Figure 1, B). The comigration of the samples (native and Cu^{II}–apoferritins) indicates, first, that the protein remained intact after reaction with Cu^{II} and, second, that the Cu^{II} atoms are indeed bound to the protein shell. The copper concentration of the mixed apoferritin-containing fractions, measured by atomic absorption, was 3.0×10^{-3} M and the apoferritin concentration, determined by the UV absorbance at 280 nm (ε^{280} = 468000 M^{-1}), was 1.08×10^{-5} M corresponding to 300 copper atoms per apoferritin.

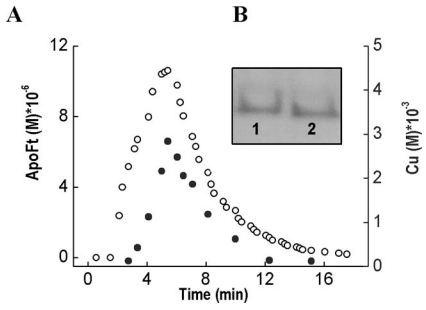

Figure 1. (A) Size-exclusion chromatography elution profile of Cu^{II}–apoferritin monitored by UV/Vis spectroscopy at 280 nm (o) and by copper atomic absorption (●). (B) Native polyacrylamide gel electrophoresis stained with Coomassie Blue: lane 1 is native apoferritin, lane 2 is Cu^{II}–apoferritin.

Interestingly, Cu^{II}–apoferritin does not react with the Cu^{II}-specific 5,10,15,20-tetrakis[4-(trimethylammonio)-phenyl]-21*H*,23*H*-porphine tetratosylate (TTMAPP), traditionally used to detect Cu^{II}. Cu^{II}–apoferritin and TTMAPP were incubated together at two different temperatures (25 and 40 °C) and the characteristic TTMAPP–Cu^{II} band at 432 nm did not increase with time. Although some radicals (7–9 Å in diameter) may slowly enter the apoferritin cavity,[23] the lack of the TTMAPP–Cu^{II} interaction can be explained on the basis of the size of the apoferritin channel (≈4 Å), which precludes the uptake of the large (≈18 Å) TTMAPP ligand. However, Cu^{II} ions of Cu^{II}–apoferritin were reduced with $NaBH_4$, small enough to traverse the apoferritin channels, to yield zero-valent Cu^0. As a result of the reduction the UV/Vis spectrum of the solution dramatically changed showing the typical surface plasmon resonance band of nanosized metallic copper, centred at 570 nm.[18,19]

Unstained TEM images of the Cu^0–apoferritin nanoparticles show the presence of discrete electron-dense spherical cores.[18,19] The stained TEM images (with uranyl acetate) enabled the visualization of the organic apoferritin coating the metal particle (Figure 2).

On the other hand, stained and unstained TEM images of the Cu^{II}–apoferritin sample appear to have less contrast in general than those of Cu^0–apoferritin, although the presence of several small nanoparticles in the interior of apoferritin is evident (see parts B and C in Figure 2). Energy-dispersive spectroscopy of both samples of Cu^{II}– and Cu^0–apoferritin confirmed the presence of Cu inside the apoferritin (data not shown). Moreover, no Cu was detected outside the ferritin particles. The nature of the Cu^{II}–apoferritin structure, as well as other metal ions binding the apoferritin species, remains uncertain. Unfortunately, no X-ray powder

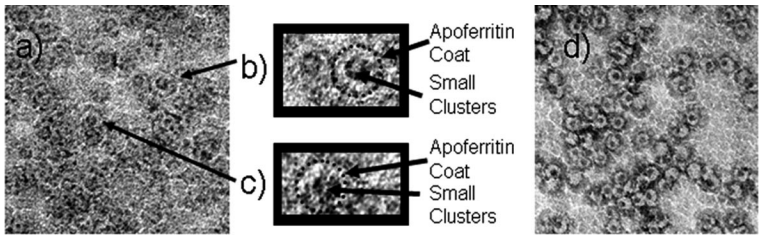

Figure 2. TEM negatively stained with uranyl acetate images: (a) Cu^{II}–apoferritin nanoparticles, scale bar 50; (b) and (c) zooms of image (a) where the apoferritin coat and the small clusters are highlighted for clarity; (d) Cu^0–apoferritin nanoparticles.

or electron diffraction could be obtained to determine the structure of the encapsulated material.

In order to gain information about the structure of the inorganic phase inside the apoferritin cavity both small angle X-ray scattering (SAXS) and X-ray absorption spectroscopy (XAS) were performed on oxidized and reduced copper–apoferritin particles.

A brief explanation of the physical origin of the SAXS signal and the meaning of the PDF curve will help us understand the results presented here. X-rays travelling through a medium with (average) uniform electron density should not deviate from their trajectory (in analogy with visible light across a medium with uniform refraction index). However, the presence of regions with different electron densities will scatter the photons rendering a size and shape specific pattern (SAXS signal). In the "infinite dilution limit", the SAXS signal is proportional to $\Delta\rho^2 = (\rho_{part} - \rho_{matrix})^2$, the excess electron density (hereinafter $\Delta\rho$) of the scatter is also the additive since every different scatter present in the sample will contribute independently to the SAXS signal.[24] The Fourier transformation of the SAXS signal produces the pair distribution function (PDF). Because of the linear properties of the Fourier transformation the PDF curve is also additive. The PDF curve can also be regarded as the autocorrelation function of the $\Delta\rho$ of the particle.[24] In this sense, finite size particles should display a vanishing PDF above a critical maximum distance (D_{max}) that, in the case of a spherical particle, will coincide with its diameter.

The intensity of the PDF curve for the case of core-shell structures can be qualitatively divided into two regions. While below $D_{max}/2$ the PDF is dominated by $\Delta\rho$, arising from the core region, above $D_{max}/2$, $\Delta\rho$ originating in the shell structure dominates the curve.

Figure 3 shows the PDF curves obtained after a regularized Fourier transform[25] of the SAXS data (also shown as Guinier plots $\{\ln[I(q)]$ vs. $q^2\}$ for Cu^{II}–apoferritin and Cu^0–apoferritin in Figure 3) obtained for apoferritin, iron-loaded–holoferritin (Fe–holoferritin) and oxidized and reduced Cu–apoferritin (Cu^{II}–apoferritin and Cu^0–apoferritin, respectively). All the PDF curves show the form expected for finite-sized particles with $D_{max} \approx 120$ Å although signals from high molecular weight aggregates can be seen above $R = 120$ Å.

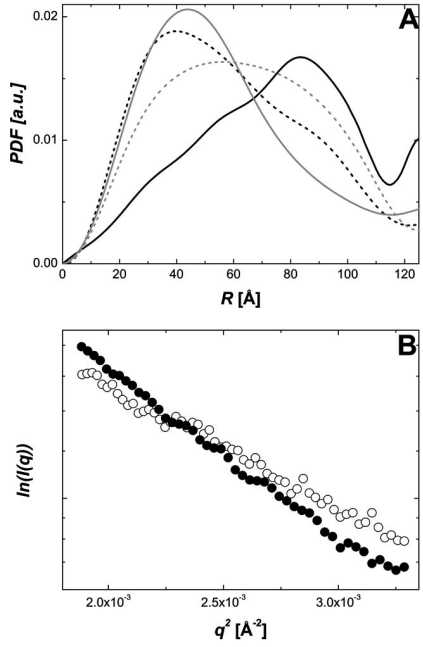

Figure 3. Pair distribution function (A) and Guinier plots (B) obtained from SAXS data for apoferritin (black full line), holoferritin (grey full line), reduced apoferritin (black dashed line and open circles) and oxidized apoferritin (grey dashed line and full circles).

The curve for apoferritin shows a maximum at high R values as expected for a spherical shell (i.e. a core-shell structure with a core that has a vanishing $\Delta\rho$). Briefly, using the argument outlined above, the area of the PDF curve bellow $D_{max}/2$ is significantly less than the area above $D_{max}/2$ suggesting that $\Delta\rho$ for the shell is greater than that for the core.

In contrast, the PDF curve for Fe–holoferritin shows a maximum displaced to lower R (lower than $D_{max}/2$) expected for the presence of a dense inorganic core (i.e. a core with a higher $\Delta\rho$ than the shell) filling the central cavity.

The PDF curve for Cu^0–apoferritin has several similarities with Fe–holoferritin. First, both curves have similar shapes indicating that Cu^0–apoferritin has, as with Fe–holoferritin, a core-shell structure with a high electron density core. Second, the maxima of both curves are almost coincident indicating that the Cu^0 core occupies the centre of the

cavity.[24] Both observations support the results derived from the TEM images indicating the presence of a compact core centred in the apoferritin cavity with high imaging contrast between the core and the shell. With regard to Cu^{II}–apoferritin, the PDF curve seems to be somewhat intermediate between a core-shell (represented by Fe–holoferritin) structure and a hollow shell sphere (represented by apoferritin). Assuming that the amount of apoferritin should not vary between both samples, a core with a lower electron density (similar to that of the shell) would explain the shape of the PDF curve.

The high sensitivity of the X-ray near edge structure (XANES) spectroscopic technique was used to gain information about the oxidation state and chemical nature of the Cu^{II}–apoferritin species. The experimental results are shown in Figure 4 together with the spectra obtained for polycrystalline CuO and $Cu(OH)_2$ used as reference materials. Grey lines correspond to the spectra obtained for the Cu^{II}–apoferritin sample (full line). Both the overall shape and structure of the spectra and their derivatives clearly indicate that the copper atoms are encapsulated as Cu^{II} species. Detailed least-squares fits of the XANES data (not shown) indicate that Cu^{II} is present as oxides and hydroxides in almost equal amounts.

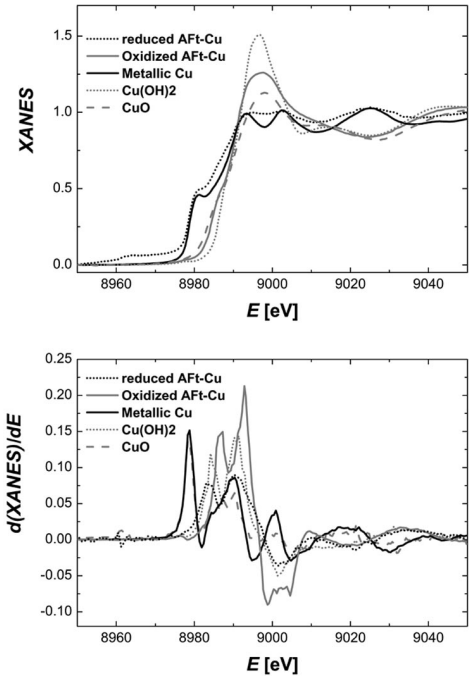

Figure 4. XANES spectra (upper panel) and their 1st derivatives (lower panel) of Cu^{II}–apoferritin (full grey line), Cu^0–apoferritin (dotted black line), metallic Cu foil (full black line), CuO (dashed grey line) and $Cu(OH)_2$ (dotted grey line).

The condensation of the inorganic phase took place at pH 8 suggesting that Cu^{II} precipitated, inside the apoferritin cavity, as an amorphous Cu^{II} oxide/hydroxide and our XANES results agree with this conclusion. To gain further structural knowledge about the Cu^{II} core we fitted the EXAFS spectra obtained from the Cu^{II}–apoferritin samples assuming an axially-distorted octahedral arrangement of the oxygen ligands around the absorber (from XAS data it is not possible to determine whether the ligands are O=, OH– or H_2O). The EXAFS data and its Fourier transform (FT) and the corresponding fitted curves are depicted in parts A and B of Figure 5, and the corresponding parameters are shown in Table 1. The quality of the fit in Figure 5 and the parameters shown in Table 1 confirm our structural model and suggest that the structural model for the Cu^{II} precursor can be described as a collection of Cu^{II} ions coordinated by six "oxygen" ligands in a distorted octahedral geometry.

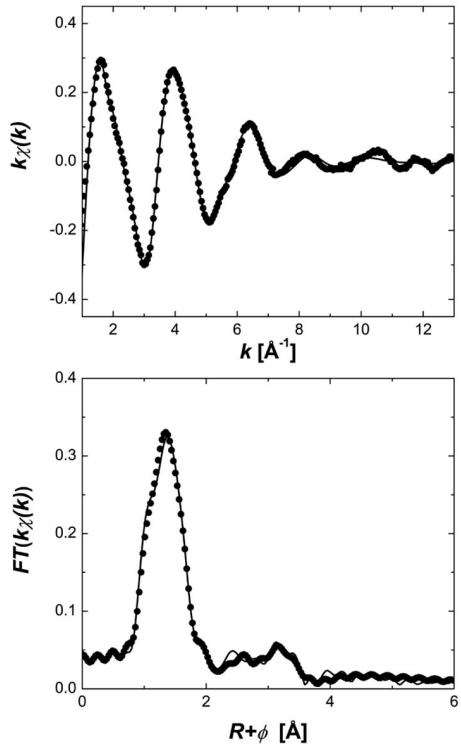

Figure 5. Upper plot EXAFS spectrum for Cu^{II}–apoferritin. Lower plot: Fourier transform of the EXAFS spectrum. Full line corresponds to the fitted curve (see text).

Table 1. Structural parameters obtained fitting the EXAFS spectrum of Cu^{II}–apoferritin. See main text for explanation.

Atom	CN	R [Å]	σ^2 [Å^{-2}]
Azimuthal O	4.3 ± 0.6	1.97 ± 0.01	$1.1 \pm 0.3 \times 10^{-2}$
Axial O	2.2 ± 0.3	2.34 ± 0.03	$1.5 \pm 0.4 \times 10^{-2}$

As already indicated the Cu^{II} oxide/hydroxide reacted with $NaBH_4$ to build a Cu nanoparticle and, after chemical reduction, the XANES spectrum (full black line) obtained for the Cu–apoferritin particles dramatically changed, resembling the one expected for metallic copper. Both the "red shift" of the position of the absorption edge and the shape of the near edge region are clearly indicative of the presence of a Cu^0 species. Moreover, attempts to detect oxidized species were unsuccessful indicating that the chemical treatment was effective in promoting the reduction of the

Cu^{II} to the Cu^0 species, confirming that full reduction of the Cu^{II} species takes place within the apoferritin nanocavity.

The evident broadening of the resonances in the XANES spectrum of the reduced apoferritin sample (compared to the resonances observed for metal copper) is due to the truncation of long scattering paths (because of the finite size of the particle) responsible for sharp oscillations in the XANES region of the spectrum.

In order to analyze the geometry around the copper atoms, EXAFS experiments were performed on Cu^0–apoferritin. Figure 6 shows the EXAFS spectra and their FTs for Cu^0–apoferritin and metallic copper. Some immediate conclusions can be drawn from the comparison between both samples. A direct comparison of the EXAFS spectra of metallic copper and the Cu^0–apoferritin sample reveals that, although similar, the atomic arrangement of Cu in the Cu–apoferritin sample can not be completely associated with a bulk FCC structure, as expected for metallic copper. The FT spectrum of Cu^0–apoferritin also shows several maxima at increasing R indicating that copper atoms in the nanoparticle occupy crystalline sites in a well-ordered structure. The amplitude of the maximum at $R_{eff} \approx 2.2$ Å is 20% lower in Cu^0–apoferritin than in metallic copper, which is compatible with a compact particle built from ca. 300 copper atoms.[26,27] Attempts to model the structure of the first coordination shell ($R_{eff} \approx 2.2$ Å) of the Cu^0–apoferritin nanoparticle with copper neighbours at about 2.55 Å in a FCC structure (as expected for metallic copper) were unsuccessful. To achieve a good fit of the experimental data, a two sub-shell model was proposed to reproduce the first coordination shell of Cu^0–apoferritin and the corresponding fitted curves can be seen in Figure 7, and the fitting parameters are shown in Table 2. It is remarkable that the coordination distance for the first sub-shell in our model (2.48 Å) coincides rather well with the first coordination distance predicted using functional density theory for the BCC phase of metallic copper.[28] The small difference between the stabilization energy observed and calculated[28] between the FCC and BCC phases of metallic copper suggests that the energy associated with the surface tension of the particle would be enough to stabilize the, otherwise unstable, Cu–BCC phase.

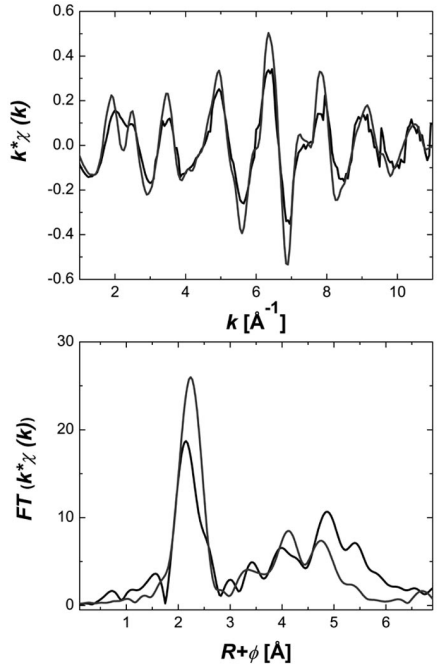

Figure 6. EXAFS (upper spectrum) and FT (lower spectrum) spectra for Cu^0–apoferritin (black line) and a metallic copper foil (grey line).

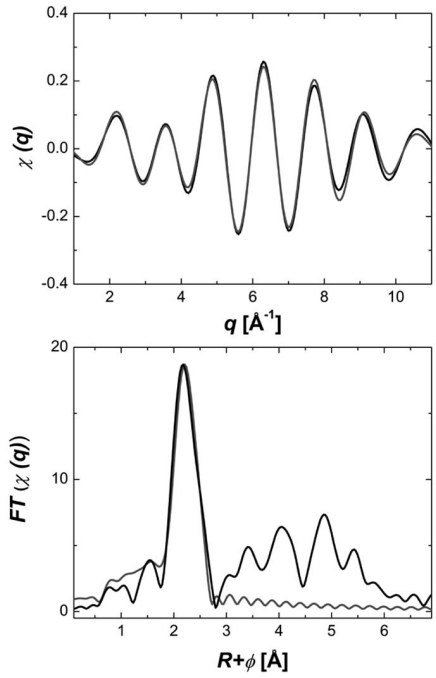

Figure 7. Back transformed (first shell) EXAFS (upper spectrum) and FT (lower spectrum) spectra for Cu^0–apoferritin (black line) and the first shell fitted curve (grey line).

Table 2. Structural parameters obtained fitting the EXAFS spectrum of Cu^0–apoferritin. See main text for explanation.

CN	R [Å]	σ^2 [Å^{-2}]
5.2 ± 0.4	2.48 ± 0.02	$1 \pm 1 \times 10^{-3}$
4.2 ± 0.5	2.62 ± 0.02	$1 \pm 1 \times 10^{-3}$

Conclusion

Previous studies using apoferritin focused on demonstrating its use for the formation of metal nanoparticles rather than investigating the nature of their precursor species. This study demonstrates that it is possible to form Cu oxide/hydroxide by direct incubation of apoferritin and Cu^{II} at high pH inside the apoferritin cavity, that it is also possible to isolate this species and finally that it can be used as a precursor to produce a Cu nanoparticle. In fact, as demonstrated by XANES, there is a full conversion from Cu^{II} oxide/hydroxide to Cu^0 when Cu^{II}–apoferritin is treated with $NaBH_4$. On the basis of XANES, EXAFS and

TEM images of the Cu^{II}– and Cu^0–apoferritin species we succeeded in proposing a growth mechanism as outlined in Scheme 1: part of the Cu^{II} ions penetrate through the hydrophilic channels, forming small clusters of Cu^{II} oxide/hydroxide on the apoferritin cavity. The clusters are formed by a collection of octahedrally oxygen-coordinated Cu^{II} ions. Once Cu^{II} is reduced to Cu^0 the clusters are destroyed and give rise to the formation of Cu nanoparticles in the interior of apoferritin. Although similar, the structure around copper atoms in Cu^0–apoferritin cannot be, solely, explained as a FCC structure as expected for metallic copper and the EXAFS spectra for the first coordination shell suggest a mixture between the stable Cu–FCC phase and an otherwise unstable Cu–BCC phase.

Experimental Section

Horse spleen apoferritin (Sigma–Aldrich, lot. 055K7012) was incubated in the presence of EDTA (10 mM) for 1 h at 4 °C and purified in a Sephadex G-25 column, previously equilibrated with Tris-HCl buffer (20 mM) at pH 7.4, to remove loosely bound iron. The iron content was determined by atomic absorption spectroscopy and the protein content by UV/Vis spectroscopy. A ratio of 1:9 for Fe/apoferritin was obtained.

Sigma-Aldrich Horse spleen apoferritin (4×10^{-5} mmol) was incubated with Cu^{2+} metal ions (0.1 M $CuSO_4$, 0.1 mmol) and the pH was dynamically adjusted to 8 with 0.01 M NaOH, to afford a homogeneous blue solution that was dialyzed against water. The apoferritin-containing fractions were isolated by G-25 Sephadex chromatography. Addition of $NaBH_4$ (4 mg) to the blue solution of Cu^{2+}–apoferritin produced a black solution of Cu^0–apoferritin. The solution was exhaustively dialyzed against milli-Q water at 4 °C. Apoferritin was monitored by UV/Vis spectroscopy at 280 nm and Cu by atomic absorption yielding 300 Cu atoms per protein. The coelution of apoferritin and metal (Figure 3) indicates that metal ions are attached to apoferritin. The purity and stability of the Cu^{II}–protein was assessed by native PAGE. Gels were stained for protein for 1/2 hour using 0.1% Coomassie Blue in fixative 40%MeOH/10%HOAc. Gel was destained by treatment with 40%MeOH/10%HOAc to remove the background over 3 h. The solutions were finally lyophilized to yield blue-green and black powders of Cu^{2+}–apoferritin and Cu^0–apoferritin, respectively.

Cu^{II}–apoferritin (1.5 mL, 3.8×10^{-4} M in Cu) and 5,10,15,20-tetrakis[4-(trimethylammonio)phenyl]-21*H*,23*H*-porphine tetratosylate (TTMAPP) (0.1 mL, 1×10^{-3} M) were incubated together in a UV/Vis quartz cuvette at two different temperatures (25 and 40 °C). The development of the Cu^{II}–TTMAPP complexes was followed by UV/Vis spectroscopy at 432 nm using a thermospectronic UV300 spectrophotometer against reference solutions containing appropriate amounts of Cu^{II}–apoferritin. Twenty cycles of 10 min were recorded. No significant changes were observed for the absorbance signal.

Full optimization of the geometry of TTMAPP was done using the MM2 method implemented from CS Chem3D software. Once the global minimum energy structure was obtained, the diameter was calculated using ChemProp Std Server software (both programs are trademarks of Cambridge Soft Corporation, Cambridge Scientific Computing, Inc., 2001).

The samples used for the TEM study were prepared by diluting the resulting solutions with milliQ water and then placing a drop onto a carbon-coated Au grid and drying it in air at room temperature. The average particle sizes and the standard deviations were estimated from TEM image analyses of 100 particles. Electron micrographs were taken with a Philips CM–20 HR analytical electron microscope operating at 200 keV.

Both SAXS and XAS experiments were performed at the D11A-SAXS1 and D04B-XAFS1 experimental stations of the Synchrotron Light National Laboratory (LNLS), Campinas, Brazil, respectively. SAXS experiments were performed at constant temperature (22 °C) controlled using a circulating water bath. The incident wavelength was set to 1.448 Å and the sample-to-detector distance was kept at 1066 mm. The scattering pattern was detected using a gas-filled 1D detector. Each spectrum was obtained as the average of at least five independent spectra. Corrections for beam intensity, sample absorption and buffer scattering were performed following standard procedures. All XAS experiments were performed at room temperature (ca. 22 °C) in transmission geometry using a copper foil for calibration purposes. Data reduction and model fitting was performed using the programs ATHENA and ARTEMIS, respectively, from the IFFEFIT package.[29] Phases and amplitudes were calculated using FEFF6.0.[30]

Acknowledgments

Financial support from the Spanish Ministerio de Educación y Ciencia (MEC) (project CTQ2006-02840) and Junta de Andalucía (Proyecto Excelencia FQM-00425) are gratefully acknowledged. N. G. thanks the Spanish MEC for a research contract (programa Ramón y Cajal). M. C. is a staff member of Consejo Nacional de Investigaciones Científicas y Tecnológicas, Argentina and full professor of Universidad Nacional del Noroeste de Buenos Aires, Argentina. Partial financial support is acknowledged from Laboratorio Nacional de Luz Sincrotron, Campinas, Brazil (projects D04B-XAFS1-5710 and D11A-SAXS1-4329).

[1] S. Mornet, S. Vasseur, F. Grasset, E. Duguet, *J. Mat. Chem.* **2004**, *14*, 2161–2175.
[2] F. Sonvico, C. Dubernet, P. Colombo, P. Couvreur, *Curr. Pharm. Des.* **2005**, *11*, 2091–2105.
[3] B. L. Cushing, V. L. Kolesnichenko, C. J. O. Connor, *Chem. Rev.* **2004**, *104*, 3893–3946.
[4] T. Douglas, *Biomimetic Materials Chemistry*, Wiley, New York, **1996**, p. 91.
[5] T. Douglas, E. Strable, D. Willits, A. Aitouchen, M. Libera, M. Young, *Adv. Mater.* **2002**, *14*, 415–418.
[6] T. Douglas, V. T. Stark, *Inorg. Chem.* **2000**, *39*, 1828–1830.
[7] K. K. W. Wong, T. Douglas, S. Gider, D. D. Awschalom, S. Mann, *Chem. Mat.* **1998**, *10*, 279–285.
[8] M. Uchida, M. T. Klem, M. Allen, P. Suci, M. Flenniken, E. Gillitzer, Z. Varpness, L. O. Liepold, M. Young, T. Douglas, *Adv. Mater.* **2007**, *19*, 1025–1042.
[9] P. M. Harrison, P. Arosio, *Biochim. Biophys. ActaBioenerg.* **1996**, *1275*, 161–203.
[10] P. M. Proulx-Curry, N. D. Chaspeen, *Coord. Chem. Rev.* **1995**, *144*, 347–368.
[11] N. D. Chasteen, *Iron transport and storage in microorganisms, plants and animals*, Marcel Dekker, New York, **1998**, p. 498.
[12] Y. Li, W. Kim, D. Wang, H. Dai, *Appl. Phys. A: Mater. Sci. Process.* **2002**, *74*, 325–328.
[13] M. Allen, D. Willits, M. Young, T. Douglas, *Inorg. Chem.* **2003**, *42*, 6300–6305.
[14] M. Okuda, K. Iwahori, I. Yamashita, Y. Zhang, H. Yoshimura, *Biotechnol. Bioeng.* **2003**, *84*, 187–194.
[15] K. K. W. Wong, S. Mann, *Adv. Mater.* **1996**, *8*, 928–932.
[16] S. Pead, E. Durrant, B. Webb, C. Larsen, D. Heaton, J. Johnson, G. D. Watt, *J. Inorg. Biochem.* **1995**, *59*, 15–27.

[17] N. Galvez, P. Sánchez, J. M. Dominguez-Vera, *Dalton Trans.* **2005**, 2492–2494.
[18] N. Galvez, P. Sanchez, J. M. Dominguez-Vera, A. Soriano-Portillo, M. Clemente-Leon, E. Coronado, *J. Mat. Chem.* **2006**, *16*, 2757–2761.
[19] M. Clemente-Leon, E. Coronado, A. Soriano-Portillo, N. Galvez, J. M. Dominguez-Vera, *J. Mat. Chem.* **2007**, *17*, 49–51.
[20] D. Ensign, M. Young, T. Douglas, *Inorg. Chem.* **2004**, *43*, 3441–3446.
[21] T. Ueno, M. Suzuki, T. Goto, T. Matsumoto, K. Nagayama, Y. Watanabe, *Angew. Chem. Int. Ed.* **2004**, *43*, 2527–2530.
[22] T. Douglas, D. R. Ripoll, *Prot. Sci.* **1998**, *7*, 1083–1091.
[23] X. Yang, N. D. Chasteen, *Biophys. J.* **1996**, *71*, 1587–1595.
[24] O Glatter and O Kratky, *Small Angle X-ray Scattering*, Academic Press, London, **1982**, p. 181.
[25] D. Svergun, *J. Applied Crystallography* **1992**, *25*, 495–503.
[26] A. Frenkel, S. Frankel, T. Liu, *Phys. Scr.* **2005**, *T115*, 721–725.
[27] A. Frenkel, *J. Synchrotron. Radiat.* **1999**, *6*, 293–295.
[28] Z. Tang, M. Hasegawa, Y. Nagai, M. Saito, *Phys. Rev. B: Condens. Matter. Mater. Phys.* **2002**, *65*, 1951081–1951088.
[29] M. Newville, *J. Synchrotron. Radiat.* **2001**, *8*, 322–324.
[30] J. J. Rehr, J. Mustre de Leon, S. I. Zabinsky, R. C. Albers, *J. Am. Chem. Soc.* **1991**, *113*, 5135–5140.

Received: August 29, 2007
Published Online: December 19, 2007

